

Exposing the Oxygen-Centered Radical Character of the Tetraoxido Ruthenium(VIII) Cation $[\text{RuO}_4]^+$

Mayara da Silva Santos,^{*,[a, b]} Robert Medel,^[c] Max Flach,^[a, b] Olesya S. Ablyasova,^[a, b] Martin Timm,^[b] Bernd von Issendorff,^[a] Konstantin Hirsch,^[b] Vicente Zamudio-Bayer,^[b] Sebastian Riedel,^{*,[c]} and J. Tobias Lau^{*,[a, b]}

The tetraoxido ruthenium(VIII) radical cation, $[\text{RuO}_4]^+$, should be a strong oxidizing agent, but has been difficult to produce and investigate so far. In our X-ray absorption spectroscopy study, in combination with quantum-chemical calculations, we show that $[\text{RuO}_4]^+$, produced via oxidation of ruthenium cations by ozone in the gas phase, forms the oxygen-centered radical ground state. The oxygen-centered radical character of $[\text{RuO}_4]^+$ is identified by the chemical shift at the ruthenium M_3 edge,

indicative of ruthenium(VIII), and by the presence of a characteristic low-energy transition at the oxygen K edge, involving an oxygen-centered singly-occupied molecular orbital, which is suppressed when the oxygen-centered radical is quenched by hydrogenation of $[\text{RuO}_4]^+$ to the closed-shell $[\text{RuO}_4\text{H}]^+$ ion. Hydrogen-atom abstraction from methane is calculated to be only slightly less exothermic for $[\text{RuO}_4]^+$ than for $[\text{OsO}_4]^+$.

Introduction

The oxygen-centered radical, $\text{O}^{\bullet-}$, i.e., an oxygen ligand with a localized unpaired electron,^[1] is considered a reactive oxygen species that plays an important role in selective oxidation processes over transition metal oxides surfaces.^[2–7] In particular, transition metal oxide cations with oxygen-centered radical character are part of a remarkable group of species that can activate methane by hydrogen-atom abstraction, which is a crucial step in reaction mechanisms involving the methyl radical, $\bullet\text{CH}_3$.^[4,5,8–10]

Gas-phase oxygen-centered radicals can be formed with a transition-metal center in its highest oxidation state. A well-known example is the tetraoxido osmium(VIII) oxygen-centered radical cation, $[\text{OsO}_4]^+$.^[11,12] In its electronic ground state, the

symmetry of $[\text{OsO}_4]^+$ is predicted as D_{2d} , where the spin density of the unpaired electron is distributed over all four oxygen ligands.^[13] The tetraoxido ruthenium cation, $[\text{RuO}_4]^+$ – the lighter congener of osmium – has previously been accessed by photoionization of RuO_4 vapor.^[14–18] Photoelectron spectroscopy studies along with calculations, neglecting any structural changes in the final state, indicate that ionization of molecular RuO_4 , with its 1A_1 ground state in T_d symmetry,^[19–21] leads to the $^2T_1(1t_1^-)$ ionic state, where the nonbonding $1t_1$ molecular orbital is of oxygen 2p atomic orbital character.^[14,17] This open $(1t_1)^5$ oxygen-centered molecular orbital implies that $[\text{RuO}_4]^+$ is an oxygen-centered radical, but it has never been identified as such.

Thermal gas-phase reactions of $[\text{RuO}_4]^+$ with methane or dihydrogen could provide evidence for the oxygen-centered radical character by hydrogen-atom abstraction, but have not been performed yet. In contrast, reactions of $[\text{RuO}_n]^+$ ($n=1–3$), with methane or dihydrogen have been studied and reveal peculiar reactivity of oxido ruthenium ions: while the $[\text{RuO}]^+ + \text{CH}_4$ reaction couple generates mainly $[\text{Ru}(\text{CH}_2)]^+$ and H_2O products,^[22] $[\text{RuO}_2]^+$ and $[\text{RuO}_3]^+$ can oxidize methane to synthesis gas (syngas, $\text{CO} + \text{H}_2$),^[23] which is a remarkable reaction otherwise only observed for $[\text{PtO}_2]^+$,^[24] $[\text{ReO}_3]^+$,^[25] $[\text{RhAl}_3\text{O}_4]^+$,^[26] and $[\text{RhAl}_2\text{O}_4]^-$.^[27] There are no reports of reactivity studies or direct spectroscopic investigations of $[\text{RuO}_4]^+$, nor has $[\text{RuO}_4]^+$ been produced in the gas phase in a controlled way, e.g. by oxidation of ruthenium ions. Consequently, there is only indirect experimental information on $[\text{RuO}_4]^+$ from photoionization and photodissociation studies of RuO_4 vapor.^[14,16–18,28,29]

Here, we present a combined gas-phase X-ray absorption spectroscopy and computational study of oxido ruthenium cations, $[\text{RuO}_n]^+$ ($n=0–4$), including $[\text{RuO}_4]^+$, and $[\text{RuO}_4\text{H}]^+$. Local and element-specific excitation at the ruthenium center or at the oxygen ligands, in contrast to valence photoelectron spectroscopy, gives independent access to the non-bonding

[a] M. da Silva Santos, M. Flach, O. S. Ablyasova, Prof. Dr. B. von Issendorff, Prof. Dr. J. T. Lau
Physikalisches Institut
Albert-Ludwigs-Universität Freiburg
Hermann-Herder-Straße 3, 79104 Freiburg (Germany)

[b] M. da Silva Santos, M. Flach, O. S. Ablyasova, M. Timm, Dr. K. Hirsch, Dr. V. Zamudio-Bayer, Prof. Dr. J. T. Lau
Abteilung für Hochempfindliche Röntgenspektroskopie
Helmholtz-Zentrum Berlin für Materialien und Energie
Albert-Einstein-Straße 15, 12489 Berlin (Germany)
E-mail: mayara.da_silva_santos@helmholtz-berlin.de
tobias.lau@helmholtz-berlin.de

[c] Dr. R. Medel, Prof. Dr. S. Riedel
Institut für Chemie und Biochemie – Anorganische Chemie
Freie Universität Berlin
Fabeckstraße 34/36, 14195 Berlin (Germany)
E-mail: s.riedel@fu-berlin.de

Supporting information for this article is available on the WWW under <https://doi.org/10.1002/cphc.202300390>

© 2023 The Authors. ChemPhysChem published by Wiley-VCH GmbH. This is an open access article under the terms of the Creative Commons Attribution License, which permits use, distribution and reproduction in any medium, provided the original work is properly cited.

4d-derived orbitals of ruthenium, and to the oxygen 2p-derived molecular orbitals, which allows us to determine the nature of the oxygen ligands. The oxidation state of the ruthenium center is inferred from shifts of the excitation energy at the ruthenium M_3 edge, and we identify a clear spectral signature of an oxygen-centered singly-occupied molecular orbital in oxygen K edge X-ray absorption spectroscopy. Our results confirm that $[\text{RuO}_4]^+$, produced from a gas-phase reaction of Ru^+ and O_3 , indeed is an oxygen-centered radical.

The experiments were performed at the ion-trap endstation,^[30] located at beamline UE52-PGM of the BESSY II synchrotron radiation facility in Berlin, and computations were carried out using density functional theory (UBP86/ZORA-def2-TZVP(SARC-ZORA-TZVP), abbreviated BP86, and UB3LYP-D3(BJ)/aug-cc-pVTZ(-PP), abbreviated B3LYP) as well as RHF-UCCSD(T)/aug-cc-pVTZ(-PP), abbreviated CCSD(T), methods. Further details on experimental and computational methods are provided in the Experimental Section and as Supplementary Information.

Results and Discussion

The Nature of the Oxygen Ligand: Oxygen K Edge Spectra of the $[\text{RuO}_n]^+$ ($n=1-4$) Series

An overview of the experimental and computational oxygen K edge spectra of the $[\text{RuO}_n]^+$ ($n=1-4$) series, shown in Figure 1 along with calculated structures, labelled by their electronic ground state and symmetry, serves to illustrate how $[\text{RuO}_4]^+$ differs from the rest of the series by its distinct nature of the oxygen ligands. Two general observations can be pointed out: first, the absence of a broad O–O σ^* resonance around 540 eV from all spectra indicates the absence of oxygen-oxygen bonds for all of the $[\text{RuO}_n]^+$ ($n=1-4$) species;^[31] second, the main transitions around 530 eV, which are again observed for all four species, are identified as the signatures of oxido ligands, as previously reported in oxido manganese cations,^[31] oxido rhodium cations,^[32] or oxidometalates.^[33] Such spectral bands are assigned to final states that result from electronic excitations from the oxygen 1s orbital to molecular orbitals with M–O (M =transition metal) π^* character.^[31,32] For $[\text{RuO}_4]^+$, this spectral region shows a double structure, similar to the case of tetraoxometalates, for which these are related to transitions involving antibonding e^* and t_2^* orbitals, with π^* and mixed σ^*/π^* characters, respectively.^[33] An additional transition at lower excitation energy of 526.6 eV, labeled “n” in Figure 1, only emerges in the $[\text{RuO}_4]^+$ oxygen K edge spectrum.

Ground State and Oxygen-centered Radical Character of $[\text{RuO}_4]^+$

Our structure optimization for $[\text{RuO}_4]^+$ (cf. Supplementary Information for details) gives a ${}^2\text{B}_2$ ground state in C_{2v} symmetry. Compared to neutral RuO_4 of T_d symmetry with uniform 1.698 Å ruthenium-oxygen bond lengths at the CCSD(T)/aug-cc-pVTZ(-PP) level, for $[\text{RuO}_4]^+$ two oxygen ligands are closer to

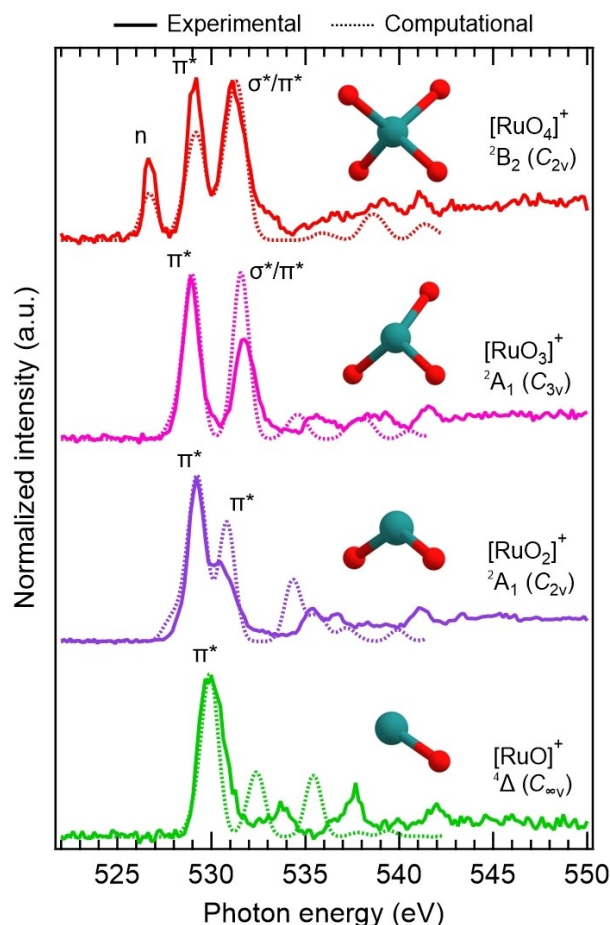


Figure 1. Experimental ion yield spectra (solid lines) and computational time-dependent density functional theory (TD-DFT, dotted lines) X-ray absorption spectra at the oxygen K edge of the $[\text{RuO}_n]^+$ ($n=0-4$) series. Higher energy transitions of computational spectra are omitted since agreement between theory and experiment is expected to be poor due to the theoretical approximations employed.^[34] The computational ground state of each molecular ion, and its respective structure (oxygen depicted in red, ruthenium in teal) are shown next to the spectra. Labels of individual final states refer to molecular orbitals of nonbonding (n), π^* , or mixed σ^*/π^* character.

the metal center, at 1.675 Å, while the other two are more distant, at 1.751 Å, see Figure 2 for the structure and numbers obtained at the BP86 level of theory, and Tables S2–S4 for the ruthenium-oxygen bond lengths of C_{2v} ${}^2\text{B}_2$ $[\text{RuO}_4]^+$ at different levels of theory. The calculated time-dependent density functional theory (TD-DFT) X-ray absorption spectrum at the oxygen K edge of $[\text{RuO}_4]^+$ shows good agreement with the experimental data, see Figure 1. Our calculations indicate that the spectral feature at 529.2 eV envelopes transitions from the oxygen 1s orbitals into π^* molecular orbitals (MOs), while the 531.2 eV feature originates from transitions into MOs with mixed σ^*/π^* character, see the corresponding MO diagram in Figure 2 for more details. The low-energy peak at 526.6 eV originates from electronic transitions that involve the oxygen spin-down 1s orbitals and the spin-down singly occupied molecular orbital (SOMO), which has nonbonding (n) oxygen 2p character, cf. Figure 2. Mulliken orbital composition analysis of the SOMO (at

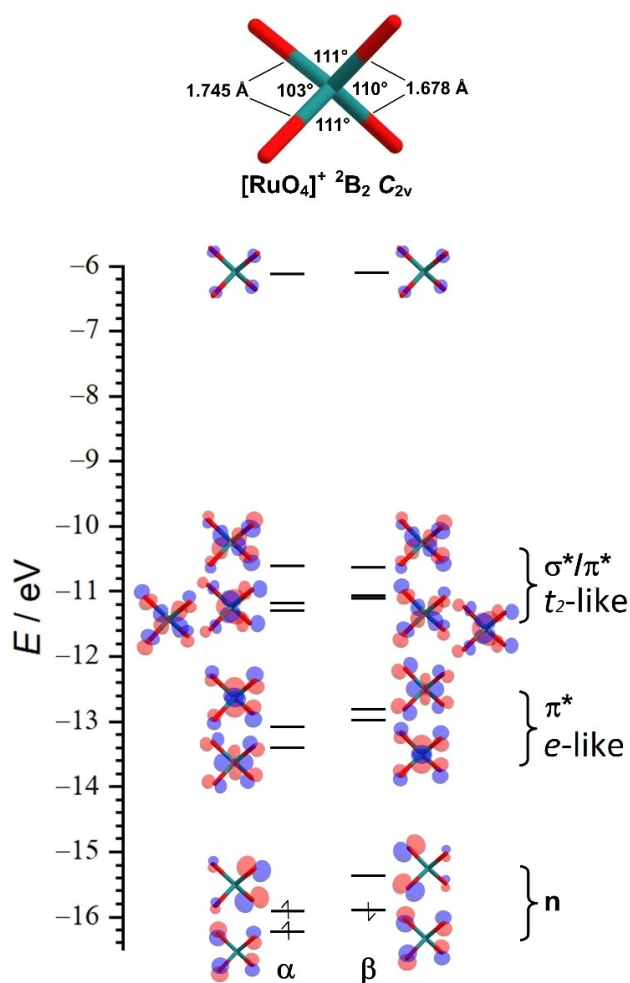


Figure 2. Upper panel: ground state structure with bond lengths and bond angles; lower panel: selected molecular orbitals (contour value 0.1) of $[\text{RuO}_4]^+$ (${}^2\text{B}_2, \text{C}_{2v}$) at BP86 level. The three experimentally observed bands at 526–533 eV are assigned to excitations involving three groups of orbitals labelled by their n , π^* , or mixed σ^*/π^* character, respectively, each at similar energy. The nonbonding (n) singly occupied molecular orbital is clearly centered at the oxygen ligands.

CCSD(T) level) quantifies 96% distant oxygen, 1% close oxygen and 3% ruthenium contribution, see Figure S9. Such localization of the SOMO at the two distant oxygen atoms gives $[\text{RuO}_4]^+$ an oxygen-centered radical character. Hence, the low-energy transition at the oxygen K edge is assigned here as the spectroscopic signature of an oxygen-centered SOMO.

All three computational methods employed here, BP86, B3LYP and CCSD(T), agree on C_{2v} symmetry for the global minimum structure of $[\text{RuO}_4]^+$. However, this C_{2v} ground state structure could also be interpreted as a distorted T_d structure, with bond distances differing by 0.06 Å from each other, and bond angles within 6° of the ideal tetrahedral bond angle. This interpretation of C_{2v} symmetry of $[\text{RuO}_4]^+$ as distorted T_d structure is also supported by the grouping of the 4d-derived orbitals into e and t_2 -like states, respectively, as shown in Figure 2. Furthermore, additional uncertainty regarding the exact geometry comes from a, likely moderate, multi-reference

character of $[\text{RuO}_4]^+$, based on T_1 and D_1 diagnostics, see Table S17.

In our study, we directly probe the oxygen-centered radical character of $[\text{RuO}_4]^+$ experimentally by the presence of the low-energy transition at 526.6 eV, related to a singly-occupied orbital localized at oxygen ligands, and reproduced in the computational spectrum. Indeed, a low-energy transition at the oxygen K edge is expected when a hole at the oxygen ligand is created.^[35] Such pre-edge peak has been assigned to electron holes at oxygen sites in intercalated cathode materials,^[35] as a signature for transitions into electron hole states with oxygen character in hematite,^[36,37] in iridium oxide^[38] electrodes for water splitting, and in strontium-doped La_2CuO_4 ,^[39] as well as a signature of H_2O^+ and OH radicals, which possess open oxygen 2p subshells.^[40] Correspondingly, electron removal from carbon 2p-derived states results in a pre-edge transition at the carbon K edge of intercalated graphite.^[41] Similarly, the emergence of a pre-edge feature upon oxidation of the ligand has previously been observed in the sulphur K edge spectra of bis(dithiolene)nickel complexes^[42] and in the nitrogen K edge spectra of a pincer-ligand-supported nickel complex with a nitrogen-centered radical.^[43] Here, this transition clearly indicates the oxygen-centered radical character of $[\text{RuO}_4]^+$.

The lowest-energy non-oxygen-centered-radical isomer of $[\text{RuO}_4]^+$, C_s ${}^2\text{A}'$ dioxido-peroxido $[\text{Ru}(\text{O})_2(\text{O}_2)]^+$, is calculated to be 13 kJ mol^{-1} higher in energy than the C_{2v} ground state at the CCSD(T) level but might still be considered energetically competitive with the C_{2v} tetraoxido radical species, based on generally accepted computational uncertainties. However, the presence of this $[\text{Ru}(\text{O})_2(\text{O}_2)]^+$ isomer in our experiment can be ruled out by its calculated oxygen K edge X-ray absorption spectrum, which does not reproduce the experimentally observed low-energy transition, nor does it agree with the absence of the characteristic oxygen-oxygen σ^* transition in the experimental spectrum, cf. Figure S6.

Ground States of $[\text{RuO}_n]^+$ ($n = 1-3$)

The ground state of $[\text{RuO}_3]^+$ has previously been reported as ${}^2\text{A}_2$ (C_{3v}) without further detail,^[23] but we were unable to locate any state of this symmetry, within more than 100 kJ mol^{-1} of our ${}^2\text{A}_1$ (C_{3v}) ground state, for which the calculated oxygen K edge spectrum would agree favorably with our experimental data given in Figure 1. Two main features are observed in the spectrum of $[\text{RuO}_3]^+$, a main peak at 528.9 eV, corresponding to an oxygen 1s transition into π^* MOs, and another intense transition around 531.7 eV, corresponding to an oxygen 1s transition into MOs with mixed σ^*/π^* character. Such double-peak structure resembles the spectra of the trioxido manganese cation, $[\text{MnO}_3]^+$ (${}^1\text{A}_1, \text{C}_{3v}$),^[31] and of the trioxidorhodium cation, $[\text{RhO}_3]^+$ (${}^1\text{A}_1', \text{D}_{3h}$), both with two main lines at 528.2 and 530.8 eV in their oxygen K edge spectra,^[31,32] where for $[\text{RhO}_3]^+$ they are assigned to oxygen 1s transitions into e'' (with π^* character) and e' (with σ^*/π^* character) MOs.^[32]

The ground state of $[\text{RuO}_2]^+$ has been reported as ${}^2\text{A}_1$ (C_{2v}),^[23] which we find nearly degenerate with a ${}^2\text{B}_1$ (C_{2v}) state

that is within ± 4 kJ mol⁻¹ of the ²A₁ state, depending on the computational method (cf. Tables S12–14). The calculated oxygen K edge spectra for both states are almost indistinguishable and agree equally well with the experimental data, cf. Supplementary Information. In Figure 1 we show the spectrum of the ²A₁ [RuO₂]⁺ state, which is the global minimum at both, CCSD(T) and BP86, levels of theory. The two main features at 529.2 and 530.6 eV correspond to oxygen 1s excitations into π^* MOs.

The ground state of [RuO]⁺ is controversial, with different reports concluding ²I_g,^[44] ⁴ Δ ,^[45] or ⁶ Σ^+ states.^[22] Here, we determine the ⁴ Δ state as the global minimum, the calculated spectrum of which is presented in Figure 1. Our computational spectra for the different states of [RuO]⁺ share the same pattern, with one main feature that corresponds to an oxygen 1s excitation into π^* MOs (cf. Supplementary Information).

The Ruthenium M₃ Excitation Energy and the Oxidation State of the Ruthenium Center in [RuO_n]⁺ (n = 1–4)

Core-level spectroscopy is routinely used to determine the oxidation state of 3d transition metals, which show a linear blueshift at the L_{2,3} edges as the oxidation state of the metal center increases.^[46,47] Similar shifts are seen at the M_{2,3} edges of 4d transition metals.^[32,48] Here, we evaluate the chemical shift, observed at the ruthenium M₃ edge, along the [RuO_n]⁺ (n = 0–4) series as a function of the formal oxidation state of the ruthenium center. The experimentally determined M₃ edge median energies, the formal oxidation states, and the formal 4d occupation numbers of the ruthenium center for each species are given in Table S1. The ruthenium M₃ edge spectra of the complete [RuO_n]⁺ (n = 0–4) series are shown in Figure S4.

Our oxygen K edge analysis and our computational results, discussed above, indicate four oxido ligands and the presence of an oxygen-centered hole in [RuO₄]⁺. Hence, the ruthenium center should have the maximum formal oxidation state of +8. The plot of M₃ edge median versus formal oxidation state in Figure 3 indeed shows a linear relation when assuming an oxidation state of +8 for ruthenium in [RuO₄]⁺, with the ruthenium center in a formal electronic configuration of 4d⁰, consistent with our computational results and with the proposed structure of [RuO₄]⁺. The chemical shift observed experimentally at the ruthenium M₃ edge is 0.90 ± 0.02 eV per unit of oxidation state, which agrees well with the rhodium M₃ edge shift of 0.88 eV in the [RhO_n]⁺ (n = 0–3) series,^[32] and lies in between the value found for the molybdenum M₃ edge shift of 0.49 eV,^[48] and for the L₃ edge shift of 3d transition metals of 1–2 eV.^[49]

Quenching the Oxygen-centered Radical: Oxygen K Edge Spectra of [RuO₄H]⁺ versus [RuO₄]⁺

For osmium, the 5d congener of ruthenium, Irikura and Beauchamp showed that the reaction of [OsO₄]⁺ with CH₄ yields [OsO₄H]⁺ + CH₃.^[11] Here, when producing [RuO₄]⁺ in the pres-

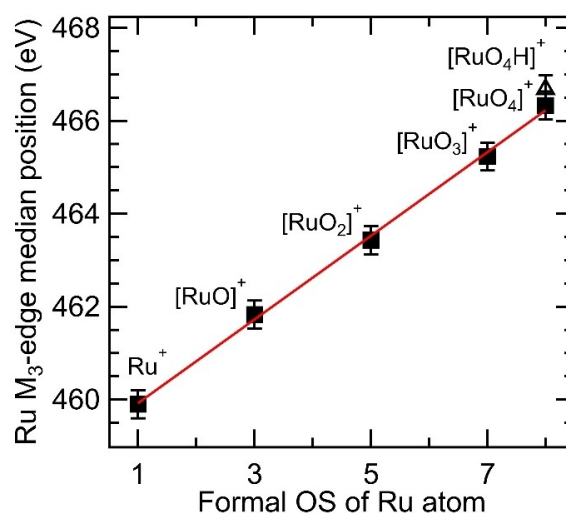


Figure 3. Median excitation energies calculated from the integrated intensity at the ruthenium M₃ edge of [RuO_n]⁺ (n = 0–4) species (solid square markers) and [RuO₄H]⁺ (empty triangle marker), plotted as a function of the formal oxidation state of the ruthenium center. The red line is a linear fit ($y = a + bx$) with coefficient values $a = 459.02 \pm 0.11$ eV and $b = 0.90 \pm 0.02$ eV per oxidation state. Cf. Table S1 for numerical values of median excitation energy.

ence of residual water vapor, we observe the appearance of [RuO₄H]⁺ in the mass spectrum, as shown in Figure S2. At room temperature, [RuO₄]⁺ might thus promote hydrogen-atom abstraction from water molecules, which we calculated to be exothermic by -21 kJ mol⁻¹, cf. Table S5. When adding CH₄ to the ion source, the [RuO₄H]⁺ isotopolog signal at $m/z = 166$ increased significantly, see Figure S2. Although our experiment was not designed for specific reactivity studies, we suggest that [RuO₄]⁺ might exhibit the same reaction pathway with methane as for its heavier congener [OsO₄]⁺, which is known to be an oxygen-centered radical. In agreement with this suggestion, our computational results indicate that hydrogen-atom abstraction from methane is highly exothermic, by -73 kJ mol⁻¹, for [RuO₄]⁺ at the CCSD(T) level, which is similar to the value of -85 kJ mol⁻¹ reported for [OsO₄]⁺.^[12] Thus, the formation of [RuO₄H]⁺ in our experiment might indicate hydrogen-atom abstraction of [RuO₄]⁺ from both, methane or water, and could be seen as another hint at the oxygen-centered radical character of [RuO₄]⁺. In addition, hydrogen-atom abstraction would again disfavor the [Ru(O)₂(O₂)]⁺ peroxide isomer, already disregarded on the grounds of both, the oxygen K edge spectrum and the oxidation state of the ruthenium center, because hydrogen abstraction would be endothermic by 37 kJ mol⁻¹ for this species, if no ligand re-arrangement takes place.

Structure optimization of the hydrogenated species, [RuO₄H]⁺, gives a global minimum structure with ¹A' (C_s) ground state, see also Tables S6–8 for the ruthenium-oxygen bond lengths of [RuO₄H]⁺ C_s ¹A' at different levels of theory. As shown in Figure 4, the characteristic low-energy transition, observed at 526.6 eV for the oxygen K edge of [RuO₄]⁺, is suppressed when the oxygen-centered radical is quenched by hydrogenation in the closed-shell [RuO₄H]⁺ ion. Instead, a shoulder at about

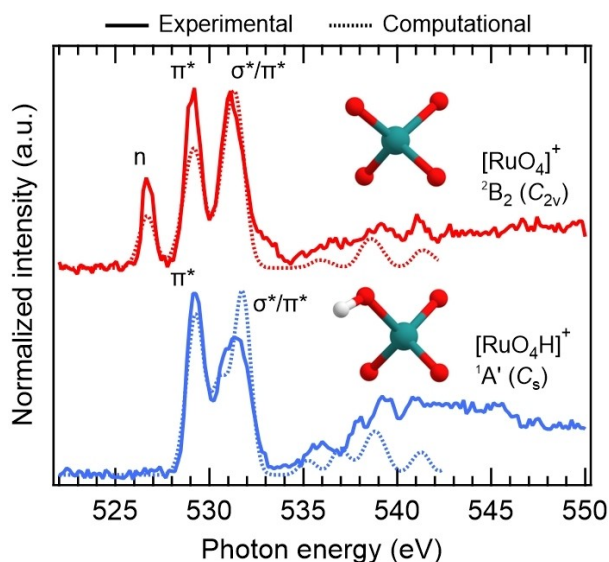


Figure 4. Experimental ion yield spectra (solid lines) and computational TD-DFT X-ray absorption spectra (dotted lines) at the oxygen K edge of $[\text{RuO}_4]^+$ and $[\text{RuO}_4\text{H}]^+$. The low-energy transition *n*, involving an oxygen-centered non-bonding molecular orbital, observed at the oxygen K edge of $[\text{RuO}_4]^+$ is suppressed when the oxygen-centered radical is quenched by hydrogenation to the closed-shell $[\text{RuO}_4\text{H}]^+$ ion. The computational ground state of each molecular ion and its respective structure (oxygen depicted in red, ruthenium in teal, hydrogen in white) are shown in the figure. Labels of individual final states are referred to in the text.

531 eV is present as a new feature in both the experimental and computational spectra of $[\text{RuO}_4\text{H}]^+$, and can be related to an increased splitting of the mixed σ^*/π^* MOs as a result of symmetry reduction to C_s .

Furthermore, the ruthenium M_3 excitation energy median of $[\text{RuO}_4\text{H}]^+$, included in Figure 3, is 466.7 ± 0.3 eV, which matches the ruthenium M_3 edge median of $[\text{RuO}_4]^+$ of 466.3 ± 0.3 eV within the error bars. Here, the 0.35 eV difference between $[\text{RuO}_4]^+$ and $[\text{RuO}_4\text{H}]^+$ ruthenium M_3 edge median is considered to be in the range of chemical shifts observed at the L_3 edge median within a same oxidation state of iron with halogen ligands of different electronegativity,^[50] as should also be the case for oxido and hydroxido ligands.^[50] Hence, the ruthenium M_3 edge median of $[\text{RuO}_4\text{H}]^+$ is consistent with the ruthenium center in the same oxidation state of +8 as in $[\text{RuO}_4]^+$, and, therefore, with the predicted structure of $[\text{Ru}(\text{O})_3(\text{OH})]^+$, since hydrogenation adds an electron to the oxygen-centered SOMO of $[\text{RuO}_4]^+$, with only little metal character, but does not induce a chemical shift at the ruthenium M_3 edge.

Conclusions

Our experimental and computational gas-phase X-ray absorption spectroscopy study confirms that $[\text{RuO}_4]^+$ is an oxygen-centered radical cation, and demonstrates a way of producing the tetraoxido ruthenium cation in the gas phase without the need for rather unstable RuO_4 vapor as a precursor. In line with our computational results, we experimentally observe the appearance of $[\text{RuO}_4\text{H}]^+$ from the reaction of oxido ruthenium

ions with CH_4 , suggesting that $[\text{RuO}_4]^+$ might exhibit hydrogen-atom abstraction, similar to the $[\text{OsO}_4]^+$ oxygen-centered radical cation of its congener, osmium. RuO_4 , as well as the ruthenates $[\text{RuO}_4]^{2-}$ and $[\text{RuO}_4]^-$, are known as oxidizing agents.^[51–62] Based on our results for the model reaction of hydrogen-atom abstraction from methane, $[\text{RuO}_4]^+$ should have an oxidizing power comparable to, or only slightly weaker than, $[\text{OsO}_4]^+$, also making it a potentially strong oxidizing agent.

We determine the chemical shift at the ruthenium M_3 edge to be 0.90 ± 0.02 eV per unit of formal oxidation state, similar to the values for $[\text{RhO}_n]^+$ M_3 and $[\text{MnO}_n]^+$ L_3 edge excitations.^[31,32] The low-energy transition at the oxygen K edge of $[\text{RuO}_4]^+$, assigned to an oxygen 1s core excitation into an oxygen-centered SOMO, is taken as the spectroscopic signature of the oxygen-centered radical. We demonstrate that the radical character is quenched for the closed-shell $[\text{RuO}_4\text{H}]^+$ species with the disappearance of such low-energy transition. In bulk samples, $[\text{RuO}_4]^+$ could probably only exist as a short-lived reactive intermediate, which would be difficult to observe experimentally. Here, gas-phase spectroscopy has the clear advantage of being able to prepare these highly reactive species for spectroscopic investigation, and opens a route to further explore gas-phase reactivity of $[\text{RuO}_4]^+$ in detail.

Experimental Section

Synthesis and Characterization

The $[\text{RuO}_n]^+$ ($n=0-4$) molecular ions were produced by argon sputtering of a ruthenium target in the presence of oxygen in the buffer gas, which was introduced as a mixture of 1% oxygen in helium 6 N. The cationic species are directed to a quadrupole mass filter, where the ions of interest are selected. The mass selected ions are guided into a linear radio frequency quadrupole ion trap, which is cooled with liquid helium to a typical temperature of 11 K.^[63] The ion trap axis is aligned with the beamline, allowing for the interaction of the X-rays with the stored and cooled ions. X-ray absorption by the parent ions is followed by an Auger cascade leading to the dissociation of the ions due to Coulomb repulsion and residual internal energy. The ion yield spectrum, representing the X-ray absorption cross section, is obtained by monitoring the product ion intensity, with a time-of-flight mass spectrometer, while scanning the photon energy over an absorption edge. The incident photon energy was scanned in steps of 160 meV with a photon energy bandwidth of 340 meV at the oxygen K edge and steps of 120 meV with a photon energy bandwidth of 240 meV at the ruthenium M_3 edge. At every photon energy step, an X-ray photoionization-photofragmentation mass spectrum is recorded.

Computational Chemistry

Search for geometric and electronic isomers was initially conducted at the spin-unrestricted B3LYP^[64–67] level with Grimme's D3 dispersion correction with two-body terms and Becke-Johnson damping^[68] and employing the aug-cc-pVTZ^[69,70] basis set for oxygen and hydrogen as well as aug-cc-pVTZ-PP^[71] for ruthenium using Gaussian 16 Rev. A.03^[72] (the method is abbreviated throughout the text as B3LYP). To obtain more accurate geometries and relative energies, low-lying isomers were reoptimized at the RHF-UCCSD(T) level employing the same aug-cc-pVTZ-(PP) basis set

using Molpro 2019.1^[73,74] (abbreviated as CCSD(T)). For subsequent calculation of X-ray absorption using time-dependent density functional theory (TD-DFT), isomers were also reoptimized at the spin-unrestricted BP86^[64,75] level employing the ZORA-def2-TZVP^[76] basis set for oxygen and hydrogen, SARC-ZORA-TZVP for rhodium, and the auxiliary basis SARC/J^[77,78] using ORCA 5.0.1^[79] (abbreviated as BP86). Molecular orbital composition analysis by Mulliken method and localized orbital bonding analysis (LOBA)^[80] was conducted with Multiwfn^[81] 3.8(dev).

Supporting Information

The authors have cited additional references within the Supporting Information.^[82–84]

Author Contributions

MSS, JTL, and VZB devised the experimental project and prepared the beamtime proposal along with MF, OSA and KH. Bvl, JTL, KH, MT, and VZB designed the experimental setup. Bvl and JTL acquired funding for its realization. MSS, MF, MT, OSA, and VZB performed the experiments and validated their reproducibility. MSS analyzed and interpreted the experimental data under guidance of JTL, KH, and VZB. JTL, KH, and VZB supervised the project. MSS wrote the original draft, with reviewing and editing by JTL, KH, VZB, RM and SR. RM performed the computational studies under guidance and supervision of SR. RM analyzed and interpreted the computational results, correlating with the experimental results along with MSS, VZB, JTL and SR. SR acquired funding for the computational studies.

Acknowledgements

Beamtime for this project was granted at the Ion Trap endstation of BESSY II, beamline UE52-PGM, operated by Helmholtz-Zentrum Berlin. This project has received funding from the German Federal Ministry of Education and Research through Grant No. BMBF-05K16VF1. Bvl, JTL, MF, MSS, and OSA acknowledge support by DFG RTG 2717. SR and RM acknowledge funding by ERC Project HighPotOx (818862). Computing time was made available by the High-Performance Computing Center at ZEDAT, Freie Universität Berlin. Open Access funding enabled and organized by Projekt DEAL.

Conflict of Interests

The authors declare no conflict of interest.

Data Availability Statement

The data that support the findings of this study are available from the corresponding author upon reasonable request.

Keywords: gas phase · ground state · oxido ligands · ruthenium · X-ray absorption spectroscopy

- [1] IUPAC, *Compendium of Chemical Terminology, 2nd Ed. (the "Gold Book")*. Compiled by A. D. McNaught and A. Wilkinson., Blackwell Scientific Publications, Online Version (2019–) Created By S. J. Chalk., Oxford, 1997.
- [2] Y. X. Zhao, X. N. Wu, J. B. Ma, S. G. He, X. L. Ding, *Phys. Chem. Chem. Phys.* **2011**, *13*, 1925–1938.
- [3] Y. X. Zhao, X. L. Ding, Y. P. Ma, Z. C. Wang, S. G. He, *Theor. Chem. Acc.* **2010**, *127*, 449–465.
- [4] H. Schwarz, P. González-Navarrete, J. Li, M. Schlangen, X. Sun, T. Weiske, S. Zhou, *Organometallics* **2017**, *36*, 8–17.
- [5] H. Schwarz, S. Shaik, J. Li, *J. Am. Chem. Soc.* **2017**, *139*, 17201–17212.
- [6] D. Johnson, G. Marston, *Chem. Soc. Rev.* **2008**, *37*, 699–716.
- [7] O. C. Williams, C. Sievers, *Appl. Catal. A* **2021**, *614*, 1–13.
- [8] Y.-X. Zhao, X.-N. Wu, Z.-C. Wang, S.-G. He, X.-L. Ding, *Chem. Commun.* **2010**, *46*, 1736–1738.
- [9] X. Ding, X. Wu, Y. Zhao, S.-G. He, *Acc. Chem. Res.* **2012**, *45*, 382–390.
- [10] N. Dietl, M. Schlangen, H. Schwarz, *Angew. Chem. Int. Ed.* **2012**, *51*, 5544–5555.
- [11] K. K. Irikura, J. L. Beauchamp, *J. Am. Chem. Soc.* **1989**, *111*, 75–85.
- [12] G. Zhang, S. Li, Y. Jiang, *Organometallics* **2004**, *23*, 3656–3667.
- [13] S. Manna, S. Mishra, *Phys. Chem. Chem. Phys.* **2020**, *22*, 628–641.
- [14] E. Diemann, A. Müller, *Chem. Phys. Lett.* **1973**, *19*, 538–540.
- [15] L. Schio, M. Alagia, D. Toffoli, P. Decleva, R. Richter, O. Schalk, R. D. Thomas, M. Mucke, F. Salvador, P. Bertoch, D. Benedetti, C. Dri, G. Cautero, R. Sergo, L. Stebel, D. Vivoda, S. Stranges, *Inorg. Chem.* **2020**, *59*, 7274–7282.
- [16] S. Evans, A. Hamnett, A. F. Orchard, *J. Am. Chem. Soc.* **1974**, *96*, 6221–6222.
- [17] P. Burroughs, S. Evans, A. Hamnett, A. F. Orchard, N. V. Richardson, *J. Chem. Soc. Faraday Trans. 2* **1974**, *70*, 1895–1911.
- [18] J. C. Green, M. F. Guest, I. H. Hillier, S. A. Jarrett-Sprague, N. Kaltsoyannis, M. A. MacDonald, K. H. Sze, *Inorg. Chem.* **1992**, *31*, 1588–1594.
- [19] P. E. M. Siegbahn, *J. Phys. Chem.* **1993**, *97*, 9096–9102.
- [20] W. Huang, W. H. Xu, W. H. E. Schwarz, J. Li, *Inorg. Chem.* **2016**, *55*, 4616–4625.
- [21] M. Filatov, D. Cremer, *J. Chem. Phys.* **2003**, *119*, 1412–1420.
- [22] X. Sun, S. Zhou, L. Yue, M. Schlangen, H. Schwarz, *Angew. Chem. Int. Ed.* **2018**, *57*, 5934–5937.
- [23] X. Sun, S. Zhou, L. Yue, M. Schlangen, H. Schwarz, *Chem. Eur. J.* **2019**, *25*, 3550–3559.
- [24] M. Brönstrup, D. Schröder, I. Kretzschmar, H. Schwarz, J. N. Harvey, *J. Am. Chem. Soc.* **2001**, *123*, 142–147.
- [25] M. K. Beyer, C. B. Berg, V. E. Bondybey, *Phys. Chem. Chem. Phys.* **2001**, *3*, 1840–1847.
- [26] Y.-K. Li, Z. Yuan, Y.-X. Zhao, C. Zhao, Q.-Y. Liu, H. Chen, S.-G. He, *J. Am. Chem. Soc.* **2016**, *138*, 12854–12860.
- [27] Y.-K. Li, Y.-X. Zhao, S.-G. He, *J. Phys. Chem. A* **2018**, *122*, 3950–3955.
- [28] J. G. Dillard, R. W. Kiser, *J. Phys. Chem.* **1965**, *69*, 3893–3897.
- [29] S. Foster, S. Felps, L. C. Cusachs, S. P. McGlynn, *J. Am. Chem. Soc.* **1973**, *95*, 5521–5524.
- [30] K. Hirsch, J. T. Lau, P. Klar, A. Langenberg, J. Probst, J. Rittmann, M. Vogel, V. Zamudio-Bayer, T. Möller, B. von Issendorff, *J. Phys. B* **2009**, *42*, 154029.
- [31] M. G. Delcey, R. Lindblad, M. Timm, C. Bülow, V. Zamudio-Bayer, B. von Issendorff, J. T. Lau, M. Lundberg, *Phys. Chem. Chem. Phys.* **2022**, *24*, 3598–3610.
- [32] M. da Silva Santos, T. Stüker, M. Flach, O. S. Ablyasova, M. Timm, B. von Issendorff, K. Hirsch, V. Zamudio-Bayer, S. Riedel, J. T. Lau, *Angew. Chem. Int. Ed.* **2022**, *61*, e202207688.
- [33] S. G. Minasian, J. M. Keith, E. R. Batista, K. S. Boland, J. A. Bradley, S. R. Daly, S. A. Kozimor, W. W. Lukens, R. L. Martin, D. Nordlund, G. T. Seidler, D. K. Shuh, D. Sokaras, T. Tylliszczak, G. L. Wagner, T.-C. Weng, P. Yang, *J. Am. Chem. Soc.* **2013**, *135*, 1864–1871.
- [34] F. Frati, M. O. J. Y. Hunault, F. M. F. De Groot, *Chem. Rev.* **2020**, *120*, 4056–4110.
- [35] R. A. House, U. Maitra, M. A. Pérez-Osorio, J. G. Lozano, L. Jin, J. W. Somerville, L. C. Duda, A. Nag, A. Walters, K. J. Zhou, M. R. Roberts, P. G. Bruce, *Nature* **2020**, *577*, 502–508.
- [36] A. Braun, K. Sivula, D. K. Bora, J. Zhu, L. Zhang, M. Grätzel, J. Guo, E. C. Constable, *J. Phys. Chem. C* **2012**, *116*, 16870–16875.

- [37] Y. Uemura, A. S. M. Ismail, S. H. Park, S. Kwon, M. Kim, H. Elnaggar, F. Frati, H. Wadati, Y. Hirata, Y. Zhang, K. Yamagami, S. Yamamoto, I. Matsuda, U. Halisdemir, G. Koster, C. Milne, M. Ammann, B. M. Weckhuysen, F. M. F. de Groot, *J. Phys. Chem. Lett.* **2022**, *13*, 4207–4214.
- [38] V. Pfeifer, T. E. Jones, J. J. V. Vélez, C. Massué, M. T. Greiner, R. Arrigo, D. Teschner, F. Girgsdies, M. Scherzer, J. Allan, M. Hashagen, G. Weinberg, S. Piccinin, M. Hävecker, A. Knop-Gericke, R. Schlögl, *Phys. Chem. Chem. Phys.* **2016**, *18*, 2292–2296.
- [39] C. T. Chen, F. Sette, Y. Ma, M. S. Hybertsen, E. B. Stechel, W. M. C. Foulkes, M. Schulter, S.-W. Cheong, A. S. Cooper, L. W. Rupp, B. Batlogg, Y. L. Soo, Z. H. Ming, A. Krol, Y. H. Kao, *Phys. Rev. Lett.* **1991**, *66*, 104–107.
- [40] Z. H. Loh, G. Doumy, C. Arnold, L. Kjellsson, S. H. Southworth, A. Al Haddad, Y. Kumagai, M. F. Tu, P. J. Ho, A. M. March, R. D. Schaller, M. S. Bin Mohd Yusof, T. Debnath, M. Simon, R. Welsch, L. Inhester, K. Khalili, K. Nanda, A. I. Krylov, S. Moeller, G. Coslovich, J. Koralek, M. P. Minitti, W. F. Schlotter, J. E. Rubensson, R. Santra, L. Young, *Science* **2020**, *367*, 179–182.
- [41] E. J. Mele, J. J. Ritsko, *Phys. Rev. Lett.* **1979**, *43*, 68–71.
- [42] R. K. Szilagyi, B. S. Lim, T. Glaser, R. H. Holm, B. Hedman, K. O. Hodgson, E. I. Solomon, *J. Am. Chem. Soc.* **2003**, *125*, 9158–9169.
- [43] J. T. Lukens, I. M. DiMucci, T. Kurogi, D. J. Mendiola, K. M. Lancaster, *Chem. Sci.* **2019**, *10*, 5044–5055.
- [44] I. R. Ariyaratna, N. M. S. Almeida, E. Miliordos, *Phys. Chem. Chem. Phys.* **2020**, *22*, 16072–16079.
- [45] E. A. Carter, W. A. Goddard, *J. Phys. Chem.* **1988**, *92*, 2109–2115.
- [46] G. Van Der Laan, I. W. Kirkman, *J. Phys. Condens. Matter* **1992**, *4*, 4189–4204.
- [47] F. D. Groot, *Coord. Chem. Rev.* **2005**, *249*, 31–63.
- [48] J. Chen, *Catal. Today* **1998**, *43*, 147–158.
- [49] H. Tan, J. Verbeeck, A. Abakumov, G. Van Tendeloo, *Ultramicroscopy* **2012**, *116*, 24–33.
- [50] M. Flach, K. Hirsch, M. Timm, O. S. Ablyasova, M. da S. Santos, M. Kubin, C. Bülow, T. Gitzinger, B. von Issendorff, J. T. Lau, V. Zamudio-Bayer, *Phys. Chem. Chem. Phys.* **2022**, *24*, 19890–19894.
- [51] J. M. Bakke, A. E. Frøhaug, *J. Phys. Org. Chem.* **1996**, *9*, 507–513.
- [52] L. M. Berkowitz, P. N. Rylander, *J. Am. Chem. Soc.* **1958**, *80*, 6682–6684.
- [53] P. H. J. Carlsen, T. Katsuki, V. S. Martin, K. B. Sharpless, *J. Org. Chem.* **1981**, *46*, 3936–3938.
- [54] J. Frunzke, C. Loschen, G. Frenking, *J. Am. Chem. Soc.* **2004**, *126*, 3642–3652.
- [55] G. Green, W. P. Griffith, D. M. Hollinshead, S. V. Ley, M. Schröder, *J. Chem. Soc. Perkin Trans. 1* **1984**, 681–686.
- [56] W. P. Griffith, *Platinum Met. Rev.* **1989**, *33*, 181–185.
- [57] W. P. Griffith, *Chem. Soc. Rev.* **1992**, *21*, 179–185.
- [58] S. Lai, C. J. Lepage, D. G. Lee, *Inorg. Chem.* **2002**, *41*, 1954–1957.
- [59] H. Petride, C. Drăghici, C. Florea, A. Petride, *Cent. Eur. J. Chem.* **2004**, *2*, 302–322.
- [60] V. Piccialli, *Molecules* **2014**, *19*, 6534–6582.
- [61] B. Plietker, *Synthesis* **2005**, 2453–2472.
- [62] C. Djerassi, R. R. Engle, *J. Am. Chem. Soc.* **1953**, *75*, 3838–3840.
- [63] A. Langenberg, K. Hirsch, A. Ławicki, V. Zamudio-Bayer, M. Niemeyer, P. Chmiela, B. Langbehn, A. Terasaki, B. von Issendorff, J. T. Lau, *Phys. Rev. B* **2014**, *90*, 184420.
- [64] A. D. Becke, *J. Chem. Phys.* **1993**, *98*, 1372–1377.
- [65] A. D. Becke, *Phys. Rev. A* **1988**, *38*, 3098–3100.
- [66] C. Lee, W. Yang, R. G. Parr, *Phys. Rev. B* **1988**, *37*, 785–789.
- [67] P. J. Stephens, F. J. Devlin, C. F. Chabalowski, M. J. Frisch, *J. Phys. Chem.* **1994**, *98*, 11623–11627.
- [68] S. Grimme, S. Ehrlich, L. Goerigk, *J. Comput. Chem.* **2011**, *32*, 1456–1465.
- [69] T. H. Dunning, *J. Chem. Phys.* **1989**, *90*, 1007–1023.
- [70] R. A. Kendall, T. H. Dunning, R. J. Harrison, *J. Chem. Phys.* **1992**, *96*, 6796–6806.
- [71] K. A. Peterson, D. Figgen, M. Dolg, H. Stoll, *J. Chem. Phys.* **2007**, *126*, DOI 10.1063/1.2647019.
- [72] M. J. Frisch, G. W. Trucks, H. B. Schlegel, G. E. Scuseria, M. A. Robb, J. R. Cheeseman, G. Scalmani, V. Barone, G. A. Petersson, H. Nakatsuji, X. Li, M. Caricato, A. V. Marenich, J. Bloino, B. G. Janesko, R. Gomperts, B. Mennucci, H. P. Hratchian, J. V. Ortiz, A. F. Izmaylov, J. L. Sonnenberg, D. Williams-Young, F. Ding, F. Lipparini, F. Egidi, J. Goings, B. Peng, A. Petrone, T. Henderson, D. Ranasinghe, V. G. Zakrzewski, J. Gao, N. Rega, G. Zheng, W. Liang, M. Hada, M. Ehara, K. Toyota, R. Fukuda, J. Hasegawa, M. Ishida, T. Nakajima, Y. Honda, O. Kitao, H. Nakai, T. Vreven, K. Throssell, J. A. Montgomery Jr., J. E. Peralta, F. Ogliaro, M. J. Bearpark, J. J. Heyd, E. N. Brothers, K. N. Kudin, V. N. Staroverov, T. A. Keith, R. Kobayashi, J. Normand, K. Raghavachari, A. P. Rendell, J. C. Burant, S. S. Iyengar, J. Tomasi, M. Cossi, J. M. Millam, M. Klene, C. Adamo, R. Cammi, J. W. Ochterski, R. L. Martin, K. Morokuma, O. Farkas, J. B. Foresman, D. J. Fox, Gaussian 16, Revision A.03, Gaussian Inc. Wallingford CT, Wallingford (United States), **2016**.
- [73] H.-J. Werner, P. J. Knowles, G. Knizia, F. R. Manby, M. Schütz, *Wiley Interdiscip. Rev.: Comput. Mol. Sci.* **2012**, *2*, 242–253.
- [74] H.-J. Werner, P. J. Knowles, F. R. Manby, J. A. Black, K. Doll, A. Heßelmann, D. Kats, A. Köhn, T. Korona, D. A. Kreplin, Q. Ma, T. F. Miller, A. Mitrushchenkov, K. A. Peterson, I. Polyak, G. Rauhut, M. Sibaev, *J. Chem. Phys.* **2020**, *152*, 144107.
- [75] J. P. Perdew, *Phys. Rev. B* **1986**, *33*, 8822–8824.
- [76] F. Weigend, R. Ahlrichs, *Phys. Chem. Chem. Phys.* **2005**, *7*, 3297–3305.
- [77] F. Weigend, *Phys. Chem. Chem. Phys.* **2006**, *8*, 1057–1065.
- [78] J. D. Rolfes, F. Neese, D. A. Pantazis, *J. Comput. Chem.* **2020**, *41*, 1842–1849.
- [79] F. Neese, *Wiley Interdiscip. Rev.: Comput. Mol. Sci.* **2022**, *12*, e1606.
- [80] A. J. W. Thom, E. J. Sundstrom, M. Head-Gordon, *Phys. Chem. Chem. Phys.* **2009**, *11*, 11297–11304.
- [81] T. Lu, F. Chen, *J. Comput. Chem.* **2012**, *33*, 580–592.
- [82] J. J. Melko, S. G. Ard, T. Lê, G. S. Miller, O. Martinez, N. S. Shuman, A. A. Viggiano, *J. Phys. Chem. A* **2017**, *121*, 24–30.
- [83] S. Reymond-Laruinaz, M. Faye, V. Boudon, D. Doizi, L. Manceron, *J. Mol. Spectrosc.* **2017**, *336*, 29–35.
- [84] J. Wang, S. Manivasagam, A. K. Wilson, *J. Chem. Theory Comput.* **2015**, *11*, 5865–5872.

Manuscript received: August 11, 2023

Revised manuscript received: August 16, 2023

Accepted manuscript online: August 17, 2023

Version of record online: September 19, 2023